Flow field assessment of the ONERA L1 wind tunnel based on numerical simulations

Geoffrey Tanguy
Univ. Lille, CNRS, ONERA, Arts et Metiers Paris Tech, Centrale Lille, UMR9014 – LMFL - Laboratory of Fluid Mechanics of Lille – Kampé de Fériet,
F-59000 FRANCE

geoffrey.tanguy@onera.fr

Thomas Renaud
ONERA, University Paris Saclay
F-92190 FRANCE

thomas.renaud@onera.fr

ABSTRACT

This paper presents the numerical investigation of the flow field within the ONERA L1 subsonic wind tunnel. The study investigates the capability of the Immersed Boundary Method (IBM) to compute the flow field within the wind tunnel for closed and open test section configurations. The comparison of the IBM solutions with body fitted unstructured computations demonstrated similar flow fields. The open test section flow field including the development of the section shear layer was well captured by the IBM method. However, wall boundary layers within the closed test section and the diffuser could not be accurately reproduced with the present IBM mesh level of refinement. The use of IBM also permits to study the effects of the model support and measurement platform over the flow within the test section. This was achieved at a low computational cost thank to the combination of automatic grid generation and a dedicated flow solver.

1.0 INTRODUCTION

In recent decades, Computational Fluid Dynamics (CFD) is often used as a complement to experimental measurements to provide some characteristic and flow configurations not achievable during a wind tunnel test. Numerical simulations can also be used to investigate the effect of wind tunnel walls and supports onto the flow field and the aerodynamic coefficients [1]–[3]. Today the increasing complexity of experimental set up tends to push the model size very close to the limit of wind tunnel test sections acceptance. Numerical results integrating the geometry of the wind tunnel can help to develop correction models for the wind tunnel measurements [4]. The use of CFD simulations prior to experimental campaign has also become very common in order to obtain an overview of the flow field and identify pertinent location of where the measurements should be performed. Numerical wind tunnels results can be used to improve the flow quality and facilitate the integration of modern measurement techniques. However, the cost to compute with a desirable quality the numerical solution of a full experimental campaign including the wind tunnel remains too high. Clearly, the development of numerical wind tunnels requires new CFD methods enabling a rapid calculation of detailed wind tunnel features coupled with the exploration of multiple design parameters.

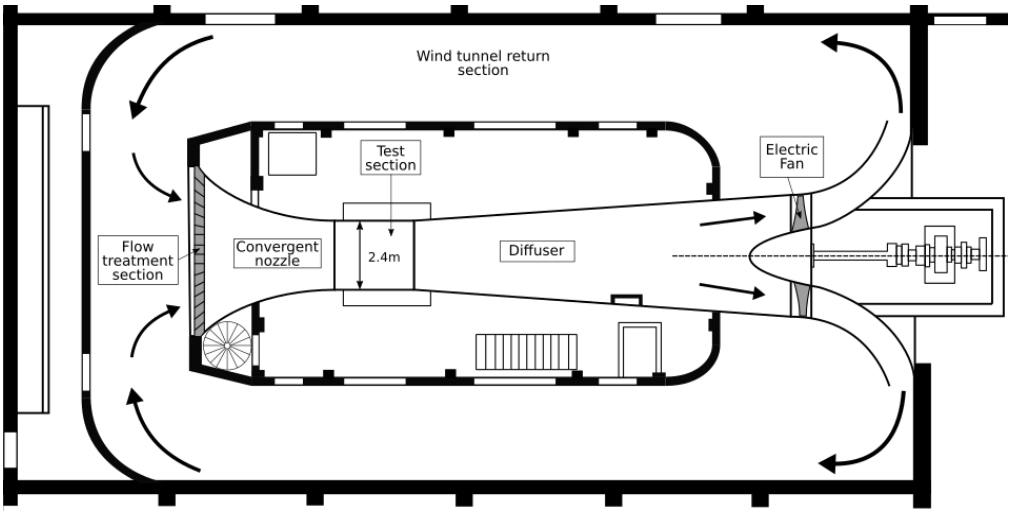

Figure 1 - Illustration of the ONERA L1 wind tunnel from the top

a) Downstream view of the closed test section in 2D configuration with a distributed propulsion wing

b) View of the open test section with PQR motorised arm with an ellipsoid model

Figure 2 - L1 open and closed test section illustrations

This paper presents an initial effort made to simulate the subsonic L1 wind tunnel for various configurations. The L1 facility at ONERA Lille is a low speed wind tunnel used for a wide variety of study from industrial to research projects. The wind tunnel can accommodate a wide range of measurement techniques from conventional forces and moments to optically based measurements. The wind tunnel can be used with either a closed or an open test section, which makes the facility highly versatile. The wind tunnel is also equipped with a 3-degree-of-freedom traverse system located downstream of the test section within the diffuser, to measure the flow field within the test section.

The aim of this work is to investigate the capability of rapid CFD calculation based on RANS modelling to replicate the empty test section flowfield of the L1 wind tunnel and assess the impact of the different wind tunnel configurations on the flow field. The simulations are carried using two different CFD methods, one based on unstructured body fitted mesh using the CFD code *elsA* [5] and the other one on Immersed Boundary Methods (IBM) coupled with the CFD code FastS [6].

2.0 ONERA L1 FACILITY

The L1 facility is a closed loop wind tunnel with a circular test section of 2.4 m diameter (D) and 2.4 m long. The flow is driven by a fan powered by a 650 kW DC electric engine. The wind tunnel occupies a 27 m long and 14 m wide hall encapsulating a 13 m height circular vault. The experimental chamber (inner part of the building) is 16 m long and 8 m wide. The inlet diameter of the wind tunnel convergent is equal to 6.50 m with a contraction coefficient of 4.31. A flow treatment section is placed within the convergent with pyramidal honeycombs to align the flow along the streamwise direction (Figure 1).

The wind tunnel can be used either with a closed or an open test section. The closed test section is made with a bespoke dodecagonal section where each face can be used with an opaque or glass panels. The closed test section can also be mounted with a series of walls to simulate the ground or provide a 2d flow (Figure 2a). Aircraft or wing models can be mounted directly on the floor (half model) or with a dedicated support. The tunnel is equipped with an external balance coupled with an angle of attack or sideslip motorized system. The open test section is used, among other available supports, with a motorised support which can provide a rotation of the model around the 3 axis (Euler angles φ, θ, ψ and rotation p, q, r). This set up can perform pitch and yaw oscillations of the model in order to acquired dynamic measurements (Figure 2b).

The wind tunnel operates at atmospheric pressure and temperature and the maximum velocity achieved within the closed test section is about 75 m/s while with the open test section, the flow can reach up to 60m/s. The operating point is controlled with four Pitot-static tubes placed within the convergent section. The dynamic pressure inside the test section is then calculated based on a calibration curve of the empty wind tunnel. Depending of the configuration investigated, the measurements corrections may include dead weight subtraction, wall/support corrections, cavity corrections and buoyancy correction. Wall and support corrections are computed using simplified potential flow modelling, solved thanks to a singularity distribution and verified using pressure measurement on the wind tunnel walls.

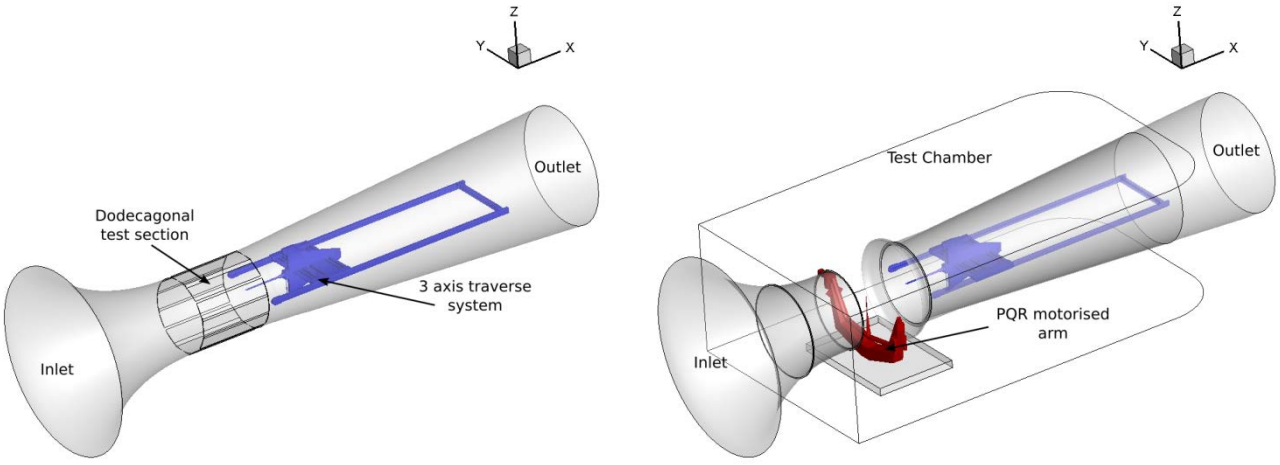

a) Closed test section configuration b) Open test section configuration

Figure 3 - Illustration of the L1 wind tunnel geometries used for the CFD calculations

3.0 NUMERICAL MODELING APPROACH

The closed and open test sections of the L1 wind tunnel are investigated in this paper as well as the effect of the 3-degree-of-freedom traverse system and the PQR motorised arm (Figure 3). For both configurations of the test section, the CFD domain includes the convergent and the diffuser of the wind tunnel. The return section of the wind tunnel is not modelled. For the open test section configuration, the test chamber and the collector are reproduced (Figure 3b). The geometry of the CFD domain is derived from the CAD files of the wind tunnel.

3.1 Description of the CFD methods

Two numerical methods are assessed for the simulation of this wind tunnel configuration. The high-fidelity CFD code *elsA*, co-owned by Airbus, Safran and ONERA [5], [7] is used as a reference solution. The *elsA* solver uses a finite volume method which consists of integrating the flow solution using a cell centred method. The solver is dedicated to the numerical simulation of the compressible viscous steady and unsteady flows, on three-dimensional structured and unstructured meshes. Its large number of numerical parameters and boundary conditions allows the accurate and robust computations of complex flows. This solver has been validated on a wide range of industrial geometries such as fixed wing, turbomachinery, rotorcraft or wind turbine configurations.

More recently, an immersed boundary method (IBM) has been developed at ONERA using a ghost cell direct forcing approach [8], [9]. The method relies on a second-order cell-centred accurate finite-volume HPC solver called FastS [6] and Cartesian structured grids which are automatically generated and locally refined around complex geometries. The pre- and post-processing steps for the immersed boundary method are performed in the ONERA Cassiopee package [10]. Musker's algebraic wall function [11] is applied within the IBM approach on Cartesian grids to solve high-Reynolds number flows. In addition, the approach has been extended to enable several types of immersed boundary conditions such as injection, outlet or slip wall. FastS contains a solver dedicated to Cartesian grids, on which we rely on to perform IBM simulations. Despite the relatively high cell count obtained by the block-structured Cartesian mesh generation in comparison with a classical body fitted unstructured approach, a dedicated Cartesian solver requires much less memory and CPU time than a structured curvilinear solver or than an unstructured solver. With these ingredients, the immersed boundary method can be seen as a good and efficient compromise between the quality of the solution and how quickly it can be obtained. With this method, the objective for the engineer is to obtain a converged solution within a day.

For both methods and solvers, present steady computations have been performed with 2^{nd}-order accurate spatial Roe-MUSCL [12] or AUSM schemes [13]. The turbulence is resolved with the Spalart-Allmaras one-equation model [14]. In terms of performance, the CPU cost of the *elsA* unstructured solver is about 4.4 µs/cells/iteration whereas the CPU cost of the FastS Cartesian solver is about 0.4 µs/cells/iteration. Generally, the unstructured mesh can require more iteration to converge, due to robustness of the solver or tricky cells for complex geometries, whereas the Cartesian IBM mesh contains isotropic and quite large cells at the wall (due to the use of wall law). For the simulation presented in this paper, the largest IBM calculation was made of 583M of cells distributed on 448 processors. As a result, a converged solution was achieved with about 15 hours of calculation.

3.2 L1 Configurations and meshes

3.2.1 Empty test section

In order to assess the capability of the Immersed Boundary Method (IBM) to capture the main flow physics in the wind tunnel, the flow field is first calculated with a body fitted unstructured mesh of the empty wind tunnel for the closed and open test sections configurations. These simulations will be used as a reference. The

unstructured mesh is made of 36 million and 25 million cells for the closed and open test section configuration respectively. The height of the wall cell size inside the wind tunnel is 5 µm which corresponds to a value of y^+ near one. The prism layer is grown over the wall in order to resolve the wind tunnel boundary layer. For the open test section, the volume mesh is also refined in the shear layer region at the convergent exhaust. The volume mesh in the test chamber is progressively coarsened to reduce the computation cost of the calculation (Figure 4a).

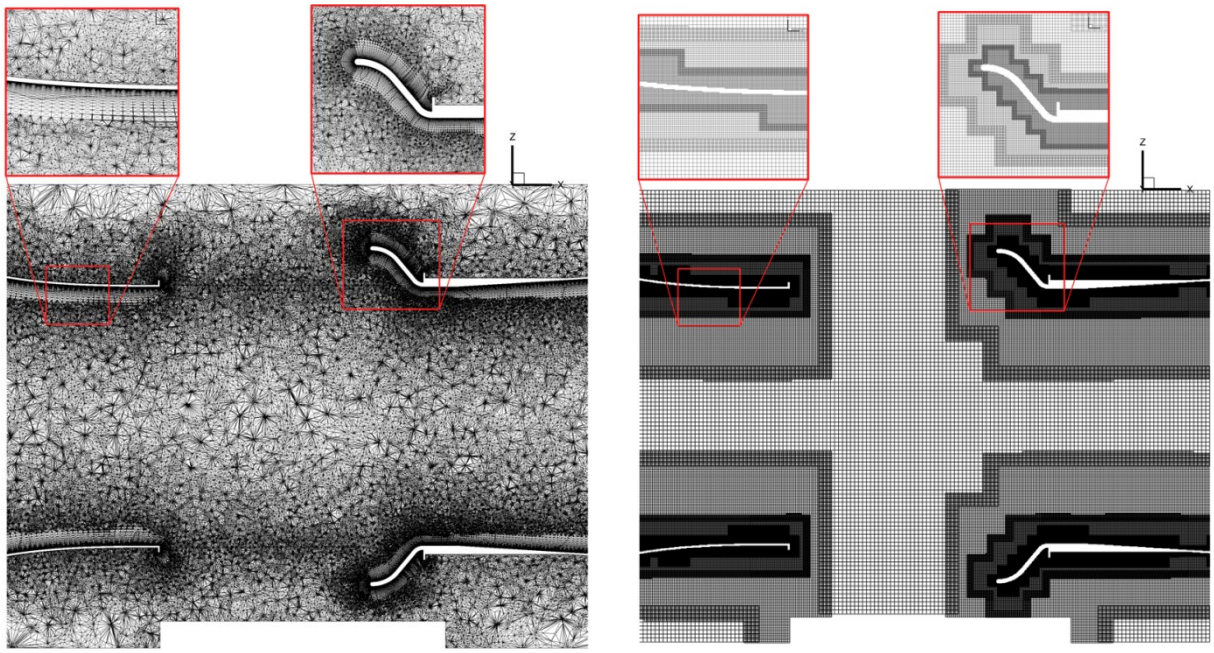

a) Unstructured body fitted mesh

b) Cartesian IBM mesh

Figure 4 - Illustration of the mesh at the symmetry plane for the empty open test section wind tunnel configuration

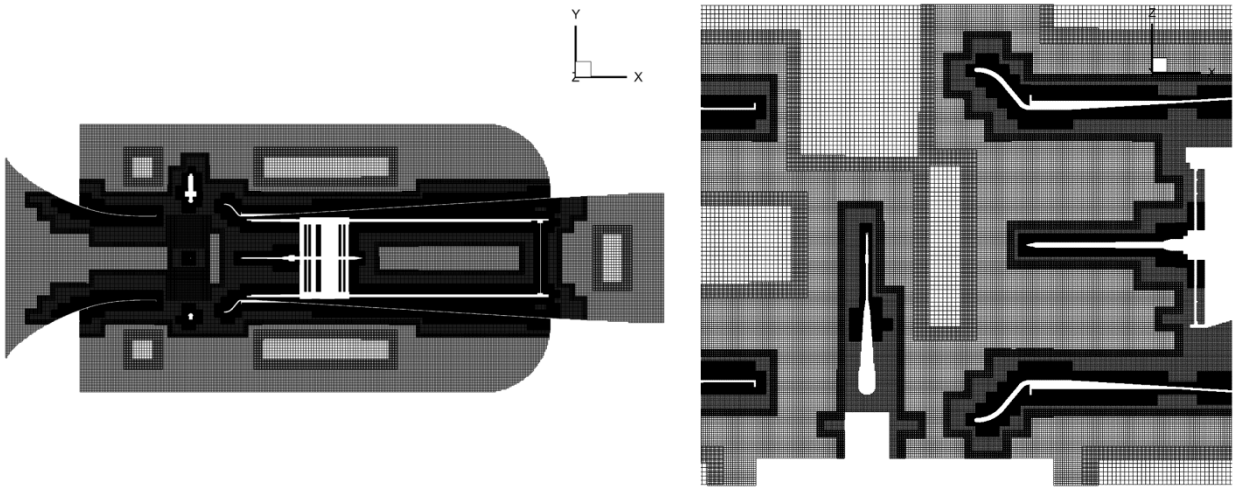

a) Middle-plane top view b) Symmetry plane

Figure 5 - Illustration of the IBM Cartesian mesh for the open test section wind tunnel configuration including the PQR and traverse system.

The volume Cartesian grid for the IBM calculation is automatically generated. The IBM uses a wall model to solve the flow field within the boundary layer. Therefore, the mesh close to the wall is not refined compared with the body fitted mesh. (Figure 4b). For the closed test section configuration, the number of cells is 152 million with a finest cell size of 6.5 mm (around the dodecagonal section steps, 13mm near wall in the convergent and diffuser sections) while, for the open test section, the cells number is 553 million for a finest cell size of 4.7mm all along the main part of the wind tunnel (in order to take into account the small thickness of the walls). For the immersed boundary method, these meshes are quite coarse and does not respect totally the range of use of the Musker wall law. The y^+ obtained with these IBM meshes is around 1000, whereas the wall function is calibrated for y^+=150.

3.2.2 Three axis traverse system and PQR model

Within the diffuser, the L1 wind tunnel accommodates a 3-axis traverse system to performed measurement of pressure and velocity at several locations in the test section based on Pitot-static probes and hot wire anemometry. The traverse platform is aerodynamically shaped. However, when the platform is placed near the diffuser inlet, a substantial flow blockage can be generated and can potentially influence the flow field within the test section. Indeed, experimental measurement demonstrated a small variation of the wall static pressure within the test section due to the location of the traverse system. However, the change of wall static pressure was mitigated when the traverse system was placed far from the test section.

The characterisation of the test section and sometimes wake surveys requires the traverse system to be placed at the inlet of the diffuser. Therefore, this paper investigates the effect of the traverse system location for two configurations. The first configuration places the traverse system at a distance X1= 1.21D from the centre of the test section, where X1 is the position of the leading edge of the horizontal platform of the traverse system and D is the test section diameter. This configuration corresponds to a typical total pressure measurement in the test section. The second configuration places the traverse system at a distance X2 =2.71D downstream inside the diffuser where its effect is supposed to be negligible.

The real geometry of the vertical and horizontal platform of the 3-axis traverse system is rather complex with a numerous appendices and details. A simplified version based on the main dimensions of the device is used instead (Figure 3a). For the closed test section configuration with traverse system, the number of cells in the IBM mesh is 192 million cells with a finest cell size of 6.5 mm (mainly on the dodecagonal test section and the traverse system).

The motorised arm "PQR" is used to vary the Euler angles (φ, θ, ψ) of a given model during an experiment. This model support can only be used in combination with the open test section due to the large dimensions of the main frame (Figure 2b). The PQR support is made of a U-shaped vertical framed which controls the sideslip angle ψ of a model and a cylindrical arm which varies the angle of incidence θ. The arm of the PQR is placed at an angle $\theta = 90°$ (vertical position) in order to match the configuration at which the open test section is characterised. For this configuration, the 3-axis traverse system in position X1 is also represented (Figure 5) thanks to the used of IBM. As a result, the mesh of the open test section including the PQR and traverse system is made of 583 million cells with a finest cell size of 4.7mm.

3.2.3 Operating and boundary conditions

Inlet boundary conditions were used at the entrance of the convergent using atmospheric uniform total pressure (100 kPa) and temperature (300°K). The outlet static pressure was tailored in order to match a velocity of 50 m/s in the central part of the test section. The outlet static pressure varied for each configuration and each CFD method. Table 1 presents a summary of the different configuration investigated in this paper.

Table 1 CFD configuration summary

#	Test section	Mesh	Solver	PQR	Traverse system	$U_\infty (m/s)$	Outlet static pressure (kPa)
CT1	Closed	Unst.	elsA	No	No	50	99.565
CT2		IBC	FastS	No	No	50	99.648
CT3				No	X1= 1.21D	50	99.420
CT4				No	X2= 2.71D	50	99.460
OT1	Open	Unst.	elsA	No	No	50	99.400
OT2		IBC	FastS	No	No	50	99.240
OT3				Yes	X1= 1.21D	50	98.870

4.0 RESULTS

4.1 Comparison between IBM and unstructured body fitted method

In order to assess the capability of the IBM to simulate the flow field of the L1 wind tunnel, a first comparison is performed with the solution calculated by the CFD *elsA* software using a body fitted fully unstructured mesh. The experimental boundary layer based on static and total pressure measurement located on the bottom surface at x/D = 0 (centre of the test section) for the closed test section is also compared with the appropriate numerical results (Figure 6).

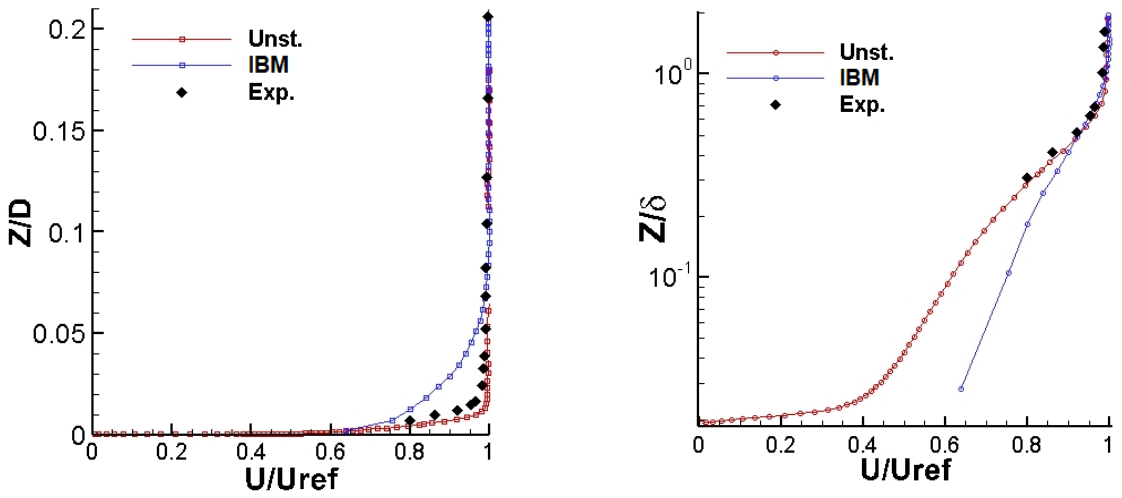

Figure 6 - Boundary layer velocity comparison on the bottom panel of the closed test section

The unstructured body fitted CFD solution slightly underestimates the boundary layer thickness (δ) compared with the experimental data (Figure 6a). However, when the height is non-dimensionalised by δ, both velocity profiles are in a very good agreement (Figure 6b). This is not the case for the solution provided by the IBM which over predicts the size of the boundary layer with δ=0.17m compared with δ=0.05m for the unstructured calculation. As expected, the IBM Cartesian mesh is not fine enough to model correctly the boundary layer with the Musker wall function [11]. Furthermore, these wall models performed poorly for boundary layers under pressure gradient. However, the test section boundary layer starts its growth inside the convergent where the flow is accelerated (Figure 7) with a strong favourable pressure gradient. As a result, the boundary layer within the test section for the IBM solution is not properly calculated.

The velocity field for the IBM and unstructured body fitted mesh calculations for the closed test section configuration is presented in Figure 7. Both CFD methods show similar flow fields. The longitudinal velocity distribution along the centre axis of the wind tunnel is also presented in Figure 9 and indicates identical results for the unstructured and IBM calculation up to 1 diameter behind the test section. Further downstream (X/D>1.5), the longitudinal velocity is reduced for the IBM solution compared with the unstructured calculation. As a result, the effectiveness of the diffuser is over predicted by the IBM which could be due to the inaccurate calculation of the boundary layer within the wind tunnel. As seen for example on Figure 5a, the IBM meshes are also coarsened far from the test section and the boundary layer is clearly not captured at the end of the diffuser.

The velocity flow field at the symmetry plane for the open test section configuration is presented in Figure 8. Both body fitted and IBM solutions are very similar in the convergent and in the open test section. However, the IBM solution predicts higher velocities along the centreline within the diffuser (Figure 9). The velocity profile in the shear layer developed at the exhaust of the convergent is very similar for the unstructured body fitted mesh and the IBM solution (Figure 10). The increase in longitudinal velocity in the collector is also present for both solutions (Figure 8).

a) *elsA* body fitted

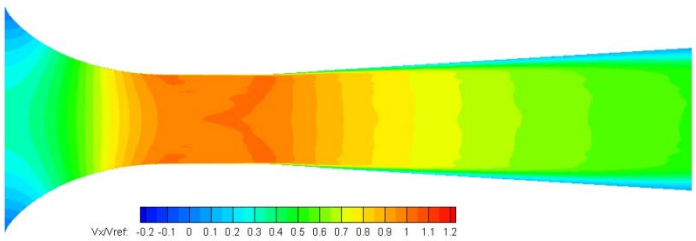

FastS IBM

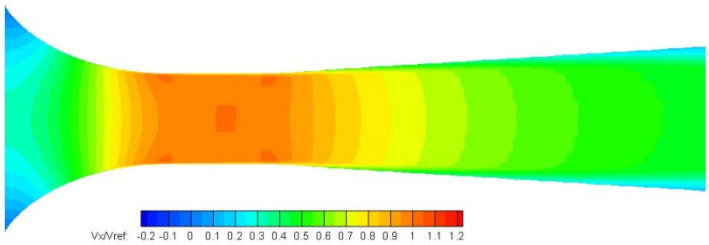

Figure 7 - Illustration of the longitudinal velocity at the symmetry plane for the closed test section wind tunnel configuration

a) *elsA* body fitted

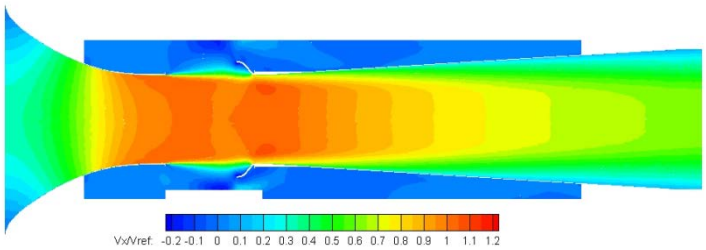

b) FastS IBM

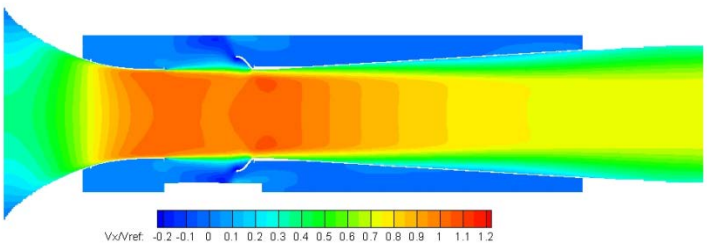

Figure 8 - Illustration of the longitudinal velocity at the symmetry plane for the open test section wind tunnel configuration

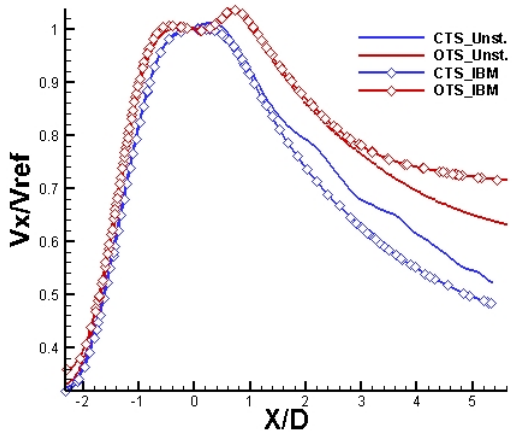

Figure 9 - Centreline velocity comparison for the closed test section (CTS) and open test section (OTS) configurations

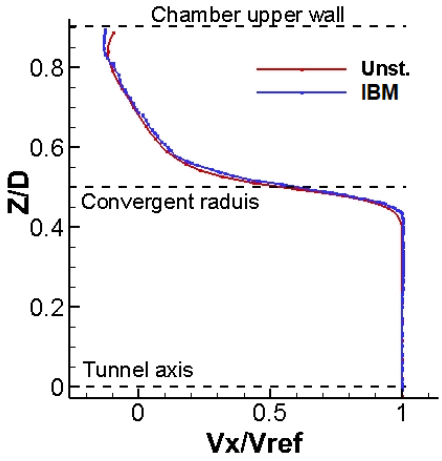

Figure 10 - Open test section velocity comparison at the symmetry plane and for X = 0 (centre of the test section)

Therefore, the comparison between IBM and unstructured body fitted mesh indicates similar results in terms of flow velocity and topology within the inner part of the test section. However, the boundary layer for the closed test section is not properly capture by the IBM calculation. For the open test section, a significant difference is present for the flow within the diffuser mainly due to the coarse Cartesian meshes used here. Nevertheless, IBM seems to be a suitable method to rapidly compute the effect of wall and model support within a wind tunnel test section.

4.2 L1 configuration flow assessment

4.2.1 Impact of the traverse system platform

The IBM is used in this section to investigate the effect of the 3-axis traverse system over the flow field of the closed test section. The position X1 and X2 of the traverse platform are investigated. The operating conditions of the simulation are made in order to match a velocity of 50 m/s at the centre of the test section.

The flow field within the wind tunnel is impacted by the presence of the platform. For the 1st configuration X1, the system is placed within a high velocity flow region providing a larger obstruction than for the 2nd configuration (Figure 11a, c). The static pressure coefficient Cp is calculated using the flow conditions in the middle of the test section as a free stream reference. The local Cp is impacted by the presence of the platform at the entrance of the diffuser (Figure 11b, d). However, the impact of the position X1 and X2 of the platform on the distribution of wall static pressure coefficient within the test section is very limited and confined primarily to the downstream portion of the section (Figure 12). The wall Cp distribution within the convergent is not impacted by the change of position of the platform from X1 to X2 (Figure 12).

One of the specificity of the L1 wind tunnel is the used of a dodecagonal test section to accommodate rectangular panel walls. The cross section in the tunnel changes from circular at the outlet of the convergent to a faceted geometry for the test section. As a result, rapid changes in the geometry are present at the junction between the test section, the convergent and the divergent. These steps and ramps are well captured by the IBM method which produces a local variation in the Cp (Figure 13).

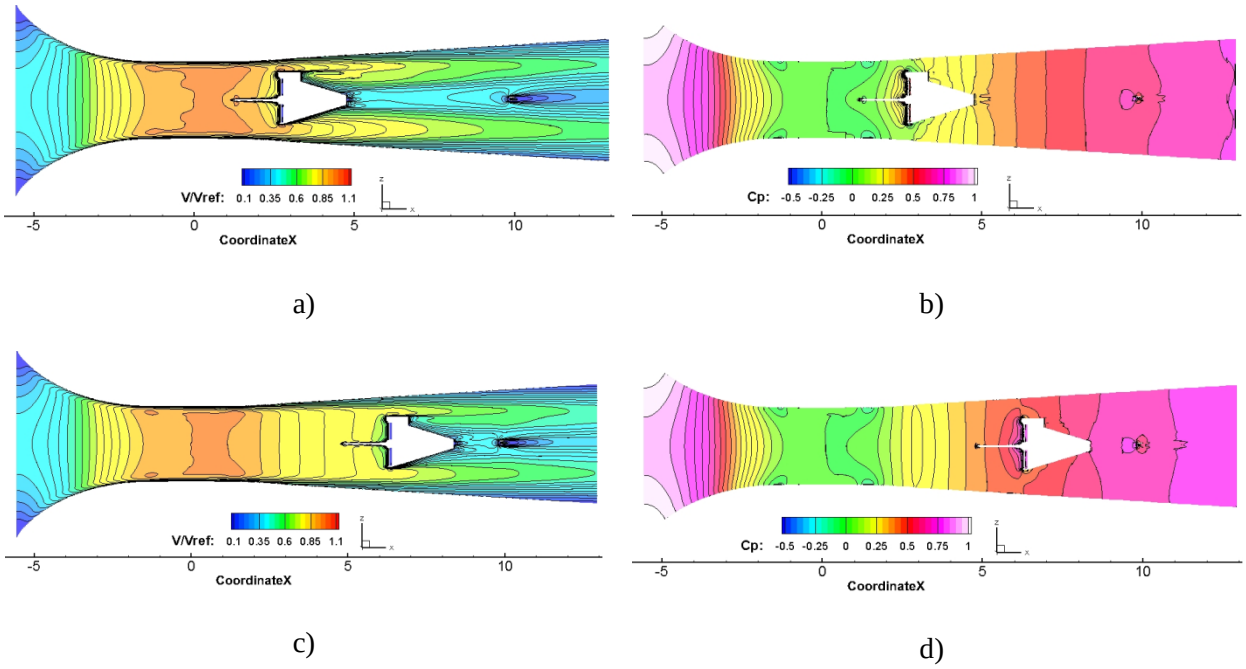

Figure 11 - Distribution of the streamwise velocity (left) and Cp (right) for both configurations X1 (top) and X2 (bottom)

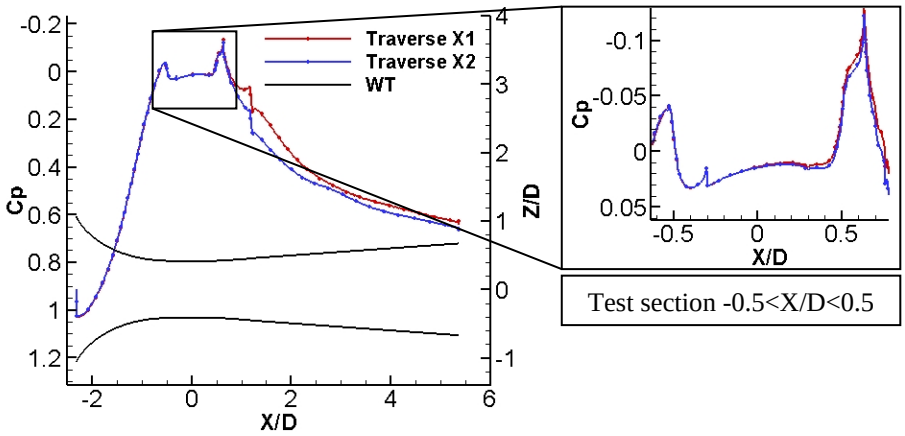

Figure 12 - Distribution of the Cp coefficient at the bottom wall of the tunnel along the symmetry plane.

a) 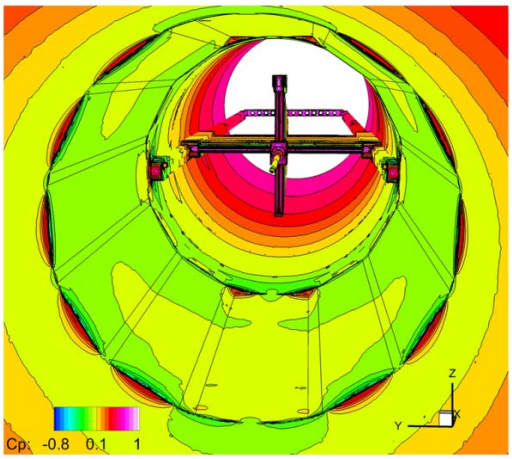

b) 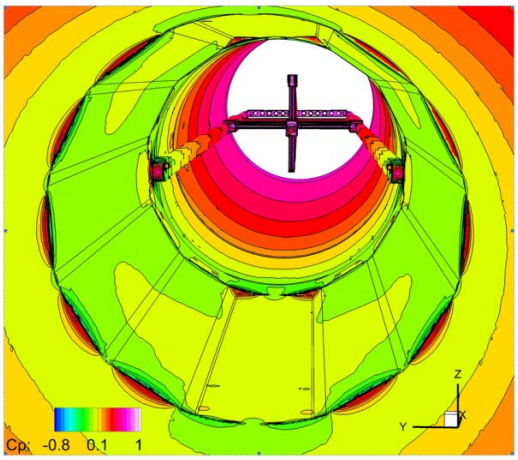

Figure 13 - Wall Cp distribution inside the wind tunnel for the closed test section and with the traverse system at the positions X1 (a) and X2 (b)

4.2.2 Impact of the PQR motorised arm

The impact of the motorised arm PQR is assessed using the IBM. In addition, the traverse system is placed at the position X1 to represent a configuration in which the test section is characterised. The static pressure flow field (Figure 14a) is affected by the presence of the PQR support in the centre part of the test section. Furthermore, a significant amount of vortical flows is developed behind the U-shaped frame which contributes to the generation of loss in total pressure ingested by the collector (Figure 14b). The presented configuration generates a pair of twin vortices which are propagated into the diffuser (Figure 15). As a result, the wall Cp distribution over the collector is non-uniform and can potentially develop high flow unsteadiness. Figure 16 shows the velocity distribution around the test section at the symmetry and middle height planes. It can be noticed that the U-shaped frame of the PQR support is outside of the convergent free jet. The assessment of the velocity distribution at the middle height plane in the test section (Figure 16b) shows a symmetric flow field despite of the non-symmetrical geometry of the U-shaped frame due to the presence of the engine located on the port side. A small portion of the jet is also redirected into the test chamber on the starboard side of the wind tunnel.

These results are the first attempt to reproduce the flow field within the open test section of the ONERA L1 wind tunnel including the PQR support. The next step of the investigation will be to place a model on the support in order to investigate the influence of the set up on the aerodynamics fields and coefficients.

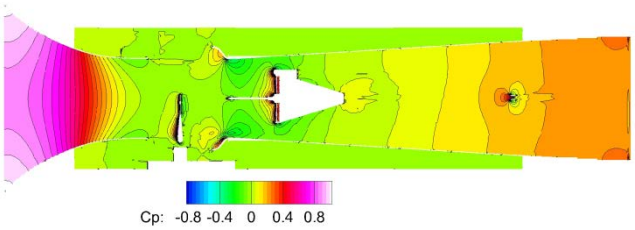

a)

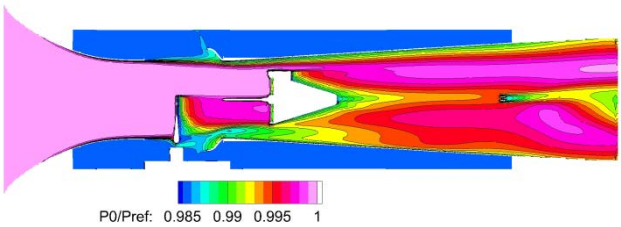

b)

Figure 14 - Distribution of the Cp (a) and total pressure (b) at the symmetry plane for the open test section configuration based on IBM results

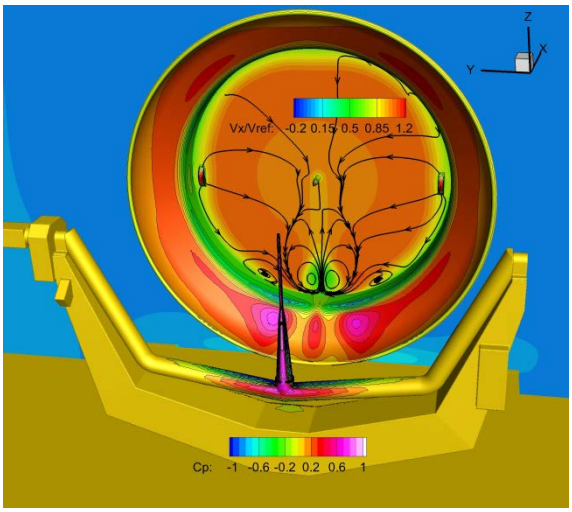

Figure 15 - Illustration of the wall Cp distribution and velocity field within the collector based on IBM results

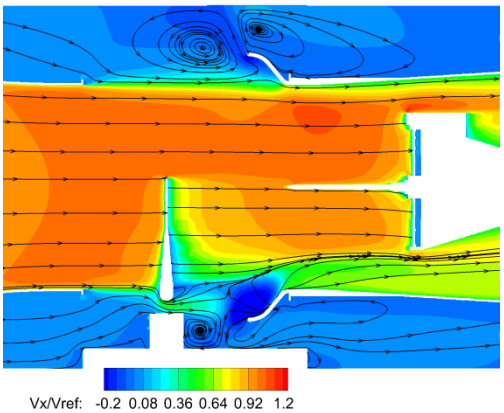

a)

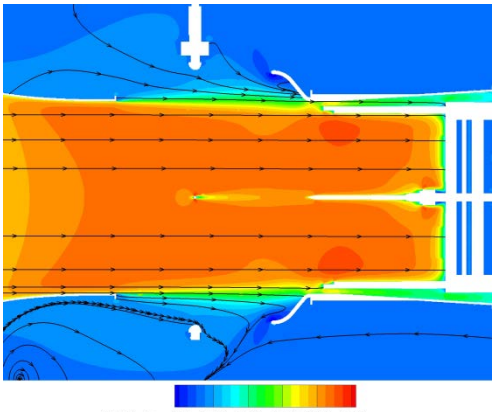

b)

Figure 16 - Distribution of the velocity at the symmetry plane (b) and mid-height plane (b) for the open test section configuration based on IBM calculation

5.0 Conclusion

This paper presents the initial results of the numerical investigation of the flow field within the ONERA L1 wind tunnel for the open and closed test section configurations. The study assessed the capability of the Immersed Boundary Method to compute an empty wind tunnel including several model and measurements support. The comparison of the IBM results demonstrates that a similar flow solution can be obtained compared with body fitted calculation. However, these solutions are obtained at a very low computational cost due to the combination of automatic grid generation and a dedicated flow solver. In the case of the open test section, the shear layer development at the exit of the convergent is well reproduced by the IBM compared with the unstructured body fitted calculation. However, it was shown that the present IBM meshes in this paper is not fine enough to compute accurate boundary layers which can today limit its use to shear flows or configuration where viscous effects are not dominant. The pursuit of this study will be done with finer meshes to correctly predict the boundary layers over all the geometry walls.

The impact of the 3 axis traverse system located in the diffuser of the tunnel was assessed. The study demonstrated a limited effect of the traverse position on the test section velocity field and the wall static pressure. The motorised arm “PQR” used with the open test section was also investigated with IBM. The results demonstrated that the support perturbs the flow field and generates non-uniformities. Therefore, these results show the potential of modern CFD tools to simulate the flow for typical wind tunnels with an affordable computational cost. However, configurations where the model support can produce high flow unsteadiness could require the use of more expensive computational tools such as hybrid RANS/LES methods to improve the flow field prediction. The tools presented in this short study will be used to support and prepare the investigation of deep stall aircraft model in open and closed test section wind tunnel.

REFERENCES

[1] Cartieri A. and Hue D., "Using RANS computations to calculate support interference effects on the Common Research Model", *STO - Meeting Proceedings Paper*, AVT-284-07, 2018, doi: 10.14339/STO-MP-AVT-284-07-PDF.

[2] Hantrais-Gervois J., and Piat J.-F., "A Methodology to Derive Wind Tunnel Wall Corrections from RANS Simulations", *STO - Meeting Proceedings Paper*, AVT-284-07, 2018, doi: 10.14339/STO-MP-AVT-284-14-PDF.

[3] Duraisamy K., McCroskey W. J., and Baeder J. D., "Analysis of wind tunnel wall interference effects on subsonic unsteady airfoil flows", *Journal of Aircraft*, Vol. 44, No 5, 2007, pp. 1683-1690, doi: 10.2514/1.28143.

[4] Wubben F. and Maseland H., "Verification of wind tunnel model support and wall interference assessments in DNW-HST by CFD simulations", *STO - Meeting Proceedings Paper*, AVT-284-05, 2018, doi: 10.14339/TO-MP-AVT-284-05-PDF.

[5] Cambier L. and Veuillot J. P., "Status of the elsA CFD software for flow simulation and multidisciplinary applications", *46th AIAA Aerospace Sciences Meeting and Exhibit*, AIAA Paper 2008-664, 2008, doi: 10.2514/6.2008-664.

[6] ONERA, "FAST: Flexible Aerodynamic Solver Technology", https://w3.onera.fr/FAST/.

[7] Cambier L., Heib S., and Plot S., "The Onera elsA CFD software: Input from research and feedback from industry", *Mechanics and Industry*, Vol.14, No. 3, pp. 159-174, 2013, doi: 10.1051/meca/2013056.

[8] Péron S., Benoit C., Renaud T., and Mary I,, "An immersed boundary method on Cartesian adaptive grids for the simulation of compressible flows around arbitrary geometries", *Engineering with Computers*, 2020, doi: 10.1007/s00366-020-00950-y.

[9] Renaud T., Benoit C., Péron S., Mary I., and Alferez N., "Validation of an immersed boundary method for compressible flows", *AIAA Scitech 2019 Forum*, AIAA paper 2019-2179, 2019, doi: 10.2514/6.2019-2179.

[10] Benoit C., Péron S., and Landier S., "Cassiopee: A CFD pre- and post-processing tool", *Aerospace Science and Technology*, Vol. 45, pp. 272-283, 2015, doi: 10.1016/j.ast.2015.05.023.

[11] Musker A. J., "Explicit expression for the smooth wall velocity distribution in a turbulent boundary layer", *AIAA Journal*, Vol. 17, No. 6, pp. 655-657, 1979, doi: 10.2514/3.61193.

[12] Roe P. L., "Approximate Riemann solvers, parameter vectors, and difference schemes", *Journal of Computational Physics*. Vol. 43, No. 2, pp. 357-372, 1981, doi: 10.1016/0021-9991(81)90128-5.

[13] Mary I. and Sagaut P., "Large eddy simulation of flow around an airfoil near stall", *AIAA Journal*, Vol. 40, No. 6, pp. 1139-1145, 2002, doi: 10.2514/2.1763.

[14] Spalart P. and S. Allmaras, 'A one-equation turbulence model for aerodynamic flows', *30th Aerospace Sciences Meeting and Exhibit*, ISBN 0034-1223, 1992, doi: 10.2514/6.1992-439